JOURNAL OF APPLIED POLYMER SCIENCE VOL. 15, PP. 2699-2731 (1971)

X-Ray Low-Angle Scattering from Oriented Poly(ethylene Terephthalate) Films

C. J. HEFFELFINGER and E. L. LIPPERT, JR.,*
E. I. du Pont de Nemours and Company,
Film Department, Circleville, Ohio 43113

Synopsis

Low-angle x-ray scattering data are used to deduce the morphology of oriented polymeric films. Generally, the structural models proposed to explain these patterns have been extrapolations of observations made from solution-grown polymer single crystals or from highly crystalline bulk polymers. These models and explanations may not be applicable broadly to oriented systems having only modest amounts of crystallinity or to those generated from precursor states that are grossly different. Poly(ethylene terephthalate) (PET) was chosen as a model polymer system for study. A systematic series of uniaxially and biaxially deformed films were produced from this polymer, made from the initially glassy or crystalline states. The low-angle x-ray scattering patterns generated from these films were studied as a function of (a) the sequence of deformation, (b) the precursor structure, (c) molecular orientation, and (d) the direction of observation. Optical diffraction and model structures were used to aid in the interpretation of the morphology produced. At least three different-sized domains are developed upon deformation, ranging from that of the unit cell (about 10 Å) to large laminar domains of average size 2,000 Å × 10,000 Å. This structure is shown to be substantially different from that developed in an oriented polyethylene film.

INTRODUCTION

Low-angle x-ray scattering data ($2\theta < 1°$) are used to deduce the morphology of films, fibers, metals, and colloidal materials. Three general types of scattering phenomena have been observed in oriented polymeric fibers and films: (a) diffuse scattering about the beam stop and at larger angles, (b) 2-point meridional diffraction, or (c) 4-point quadrant diffraction. These diffraction effects have been used to calculate a long period spacing, indicative of a periodic structure in these materials, usually >100 Å.

Several interpretations have been proposed to explain the morphology responsible for these scattering phenomena in specific polymer systems.[1-4,14] Statton[5] and Alexander[6] have reviewed these interpretations and have discussed the similarity of the scattering patterns observed from oriented films, oriented fibers, and from lamellar crystals grown in the bulk and from solution. Much morphological evidence suggests that the basic crystalline

* Present address: Owens-Illinois Inc., Corporate Research Technical Center, Toledo, Ohio 43601.

structures of oriented polymers may be related in kind but differ in detail. The properties of materials, however, are influenced by the morphological details.[7] Stress, thermal treatments, nucleation, and growth rates all influence the way a polymer will crystallize. A definitive study of polyethylene by Keller and Machin[8] has emphasized the variations in structure (e.g., the combinations of fibrous and folded chain crystalline lamellae) that can be produced, depending upon the method of sample preparation. Thermal gradients, heterogeneous nuclei, and flow during processing all markedly affect the morphology obtained in linear crystalline polymers.[9,10]

Structural interpretations based largely on x-ray and electron low-angle discrete diffraction data from spherulitic specimens and from solution-grown polymer crystals have emphasized the necessity for a folded-chain lamellar type of crystalline morphology. We find it difficult to attribute this explanation as the source for the small-angle x-ray scattering observed in very highly oriented polymer systems, such as poly(ethylene terephthalate) having low to modest crystallinity. Highly oriented materials may be produced by deforming precursor states that are substantially different, e.g., crystalline or amorphous. The structure responsible for the low-angle x-ray scattering patterns from such materials may have little or no relationship to that responsible for the scattering from spherulites or from solution-grown single crystals. Orientation adds to the complexity of developing a morphological explanation of x-ray scattering patterns. However, orientation is also a useful tool to help separate and classify the scattering effects that are produced.

Our objectives in this study were: (1) to investigate a polymer system of modest crystallinity that could be deformed from the precursor glassy or crystalline states, (2) to determine how these structures differ in their low-angle scattering relative to the type and amount of crystallite orientation as measured by wide-angle x-ray diffraction, and (3) to compare these results with those reported for oriented polyethylene film.

We chose poly(ethylene terephthalate) as a polymer to study because it can be obtained easily in either the crystalline or amorphous forms prior to deformation. In addition, the chemistry, the relatively low molecular weight ($\bar{M}_n \cong 15{,}000$), and the secondary bonding characteristics are substantially different from the aliphatic structures such as polyethylene that have been studied so intensively.

EXPERIMENTAL

Materials and Techniques

Poly(ethylene terephthalate) (PET) films were prepared from polymer having a limiting viscosity number of 0.54–0.56 dl/g measured in a 40–60 wt-% mixture of *s*-tetrachloroethane and phenol. Prior to deformation, some of the amorphous films were crystallized by annealing them for 16 hr at 140°–150°C. This time–temperature program is many half-times that required to achieve a relatively constant level of crystallinity,[11] but below a

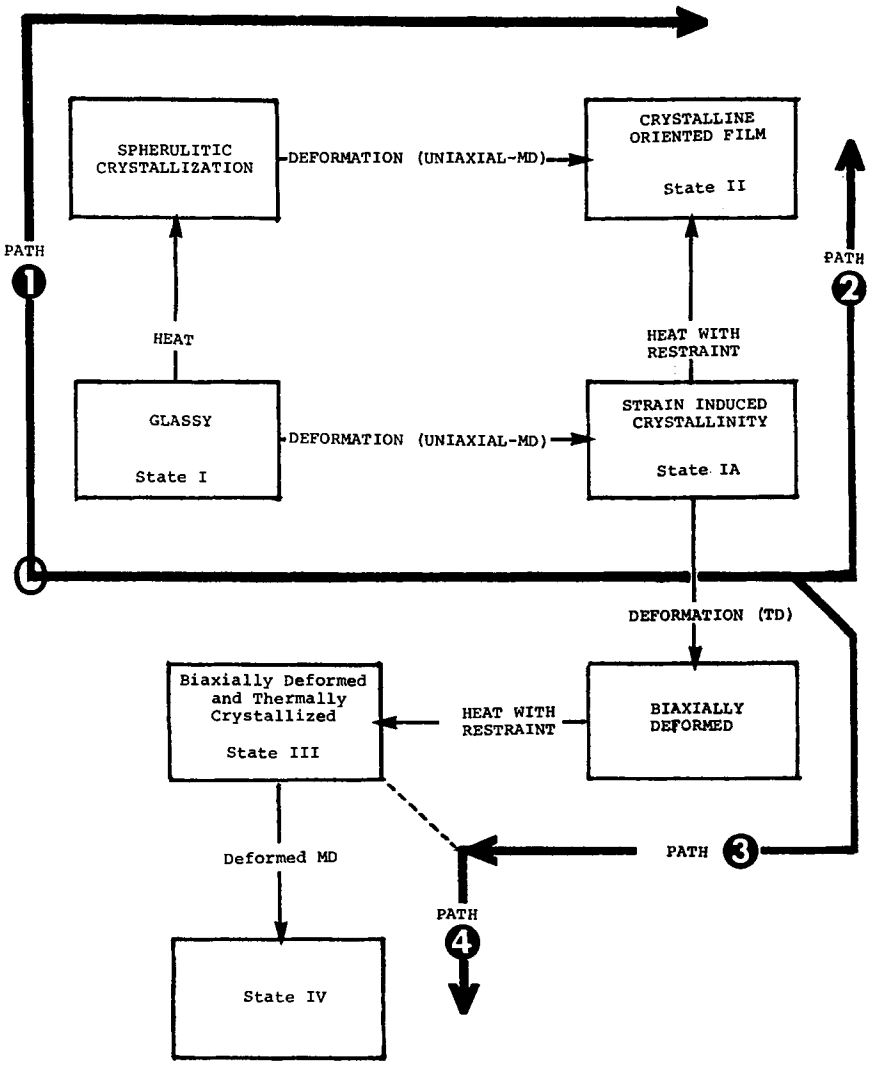

Fig. 1. Deformation paths and heat treatment conditions used in the preparation of experimental PET films.

temperature where appreciable ester interchange will occur in the solid state. The spherulites formed, as described by Keller,[12] had a positive birefringence. The sequence of deformation steps used to prepare the film structures measured are shown schematically in Figure 1. These crystalline films were deformed uniaxially (path 1). Other samples were deformed from the glass, as described previously,[7,13] below the crystallization temperature and to about the same level of crystallite orientation as the path 1 films. Samples deformed from the glass were then subsequently thermally crystallized under restraint at 140°–150°C (path 2). The film samples

produced by the two paths had equivalent molecular orientation and about the same density, a measure of crystallinity. They were made, however, from precursor structures that were substantially different.

Biaxially oriented films were prepared as illustrated in path 3 by deforming the path 2 structure at state IA in a direction normal to the first. Other samples were deformed in both directions simultaneously. These films were then annealed at 200°C with restraint (constant dimension). Path 4 involves the deformation of the path 3 structure in the direction used to achieve state IA. A discussion of the crystallite orientation distributions produced in films made according to paths 2–4 has been given previously.[7] The films reported here were 1–20 mils in thickness.

Low-angle x-ray scattering patterns were obtained using a vacuum camera at 17 and 32 cm sample-to-film distances and nickel-filtered CuKα radiation. Pinhole collimators 15 mils in diameter were used. Exposure times of 8 hr for the 17-cm and 24 hr for the 32-cm distances were employed.

Sample Geometry

Sample position relative to the x-ray beam has often been omitted in reporting the results of low-angle scattering. For anisotropic materials, the patterns obtained depend on the position of the sample with respect to the incident x-ray beam and must be specified.[5] We found the coordinate scheme shown in Figures 2a and 2b to be useful in describing the photo-

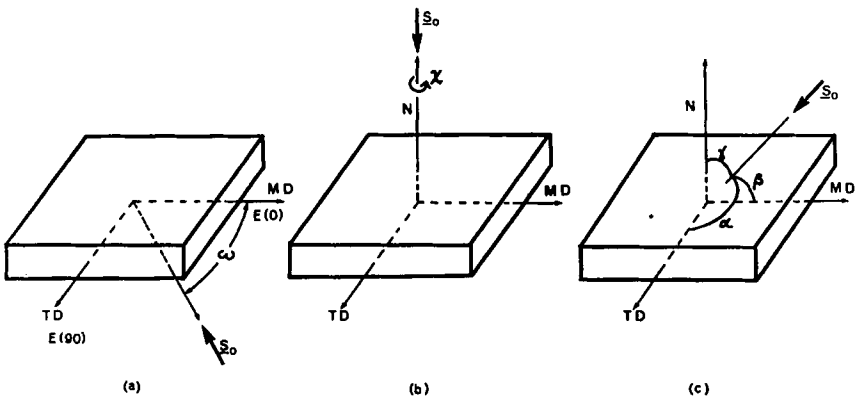

Fig. 2. (a) Definition of the angle ω used for edge low-angle scattering. (b) Definition of the angle χ used in the crystallite orientation distributions. This diagram also shows the orientation of the sample and x-ray beam (S_0) for a through, or N, low-angle photograph. (c) Definition of the Eulerian angles α, β, and γ used to specify the relative positions of the sample and the x-ray beam (S_0).

Name	E-N System	Eulerian System
MD edge photo	E(90)	E(0,90,90)
TD edge photo	E(0)	E(90,0,90)
N photo	N	E(90,90,0)

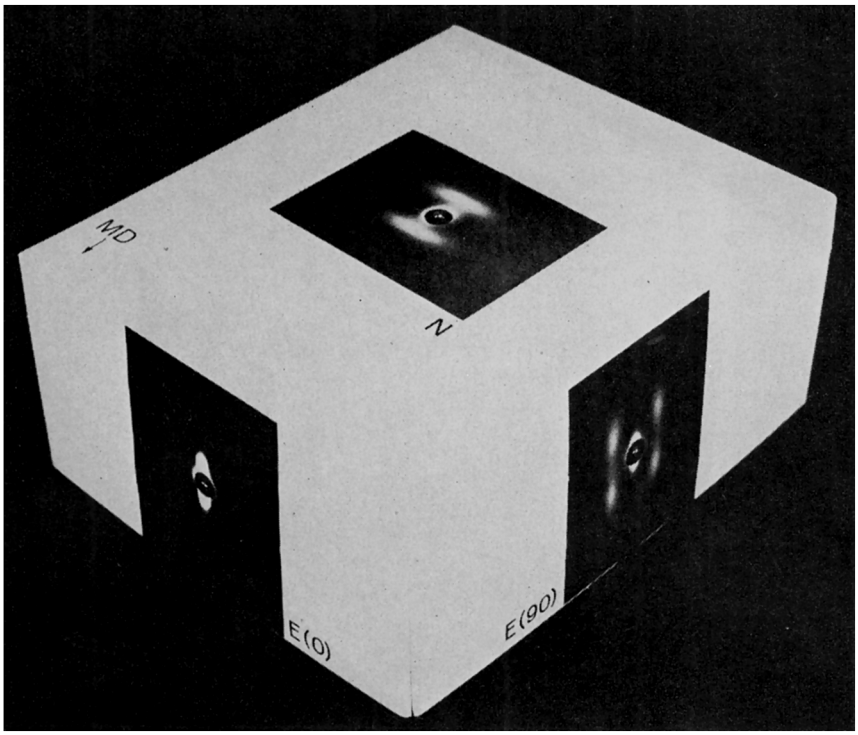

Fig. 3. Three-dimensional representation of the scattering observed for a uniaxially deformed (path 1) film prepared by deformation of a spherulitically crystallized polymer.

graphs discussed here. However, it may be necessary in some systems to utilize the three Eulerian angles to describe the direction of the incoming beam relative to the geometry of the sample, as illustrated in Figure 2c.

Our frame of reference resides in the sample. The arbitrarily chosen direction of initial deformation is taken as the machine direction (MD). An MD edge photograph, E(90), results if the x-ray beam (S_0) impinges on the film parallel to the surface and perpendicular to the MD axis. Similarly, a transverse direction (TD) edge photograph, E(0), results if the beam is perpendicular to the TD axis and parallel to the surface of the film. Intermediate positions are designated by E(ω). A through-photograph, N, results if the beam is directed normal to the surface of the film, as in Figure 2b.

Typical Scattering Patterns

Figures 3 to 6 illustrate the type of low-angle scattering patterns obtained for films prepared by the four deformation paths described in Figure 1. Figure 3 is a montage of the scattering obtained from the deformed spherulitic structure (state II via path 1), while Figure 4 is a like arrangement for films deformed from the glassy state (state II via Path 2). The scattering patterns from these structures are equivalent in kind but exhibit small dif-

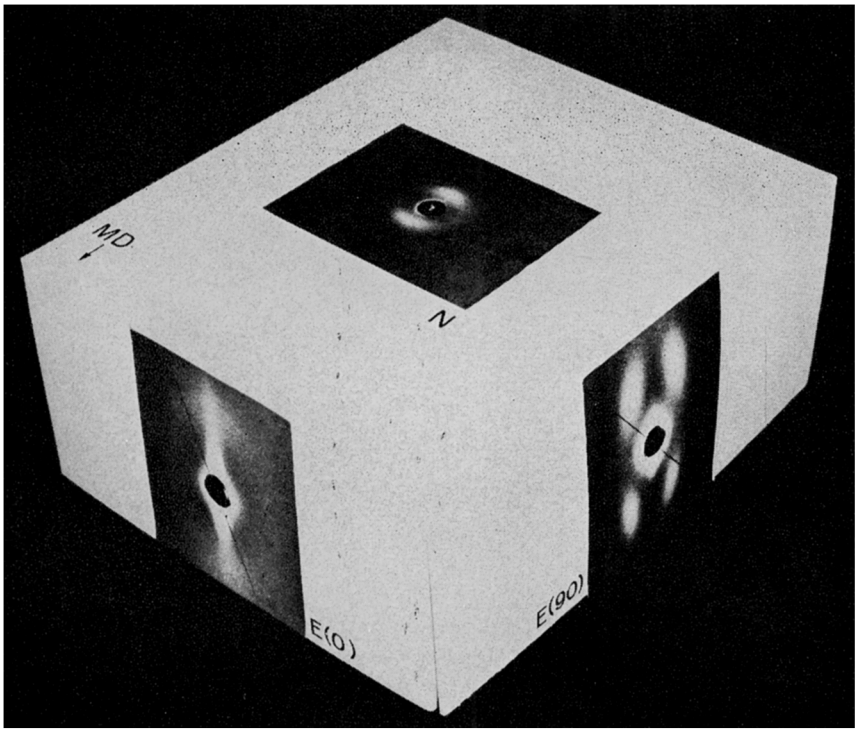

Fig. 4. Three-dimensional representation of the scattering observed for a uniaxially deformed (path 2) film prepared by the deformation of a glassy polymer followed by thermal annealing.

ferences, such as the relative intensities of the quadrant diffraction, the size of the center streak, and the shape of the N diffraction spots. The densities and the crystallite orientation measurements[13] indicate that the amount of crystallinity and the molecular orientation are essentially the same in these structures (Fig. 7).

The type of long period diffraction obtained from uniaxially oriented PET films depends upon the amount of sample deformation.[7] Typical uniaxially deformed (>250%) films exhibit scattering which have (1) a 4-point or quadrant pattern when viewed in the MD edge or E(90) position, (2) a less intense 2-point pattern when viewed in the through or N position, and (3) a very weak elliptical halo when viewed in the TD edge or E(0) position. The intensity distribution in the E(0) ellipse varies from almost zero at the equator to a maximum at the meridian. At low levels of uniplanar-axial crystallite orientation,[13] only the center streak and 2-point diffraction are observed, as shown in Figure 8.

Figure 5 is a montage of the scattering patterns obtained in the orthogonal directions from two biaxially deformed samples (path 3). A 2-point pattern is obtained in the edge views, E(0) and E(90). The N or through-position yields only a relatively weak circular halo for films of balanced

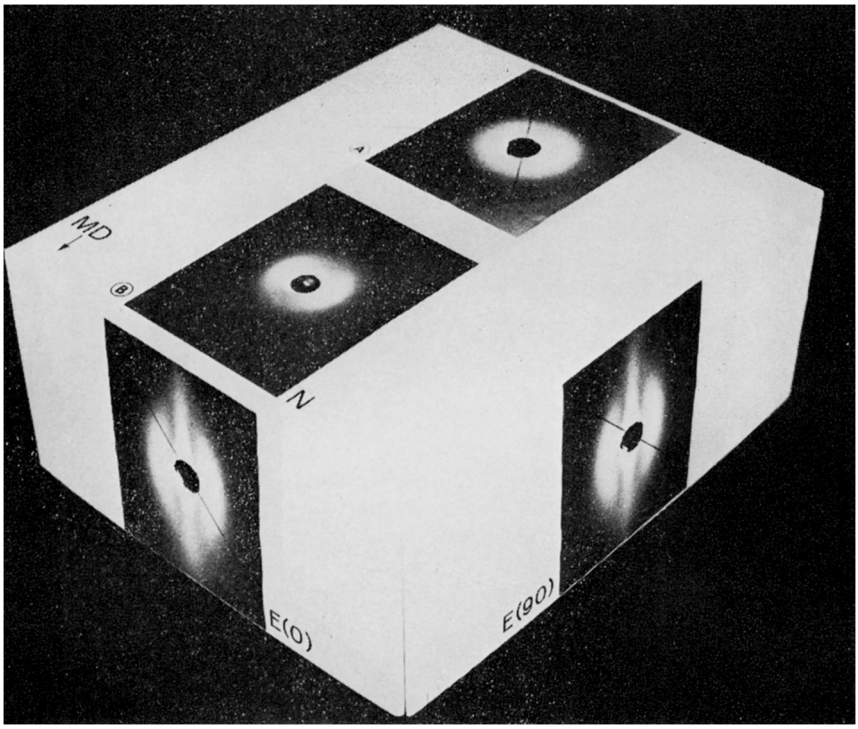

Fig. 5. Three-dimensional representation of the scattering observed for a biaxially oriented (state III via path 3) film prepared by deformation of state IA in the transverse direction followed by thermal annealing under restraint: (a) Simultaneously or sequentially deformed 250 by 250%; (b) sequentially deformed 250% MD followed by 250% TD.

crystallite orientation (Fig. 5a). Films with unbalanced orientation show weak meridional reflections in the direction of greatest deformation (Fig. 5b). Identical patterns are obtained independent of the mode of biaxial deformation, e.g., sequential or simultaneous. As with the uniaxial films, a center streak is never observed in the N scattering pattern.

The scattering patterns produced by films prepared by path 4 are shown in Figure 6. It was expected from the method of sample preparation[7] that the morphology, and hence the scattering arising from it, would be intermediate between that observed from the uniaxially deformed and from the balanced biaxial structures. The E scattering shown in Figure 6 progresses from an almost-quadrant pattern in the E(90) position to an elliptical pattern at E(0). This result, unlike the E(0) pattern in uniaxially deformed films, has weak intensity maxima both parallel and perpendicular to a direction normal to the film surface.

In contrast, we illustrate with Figure 9 the typical patterns obtained from an oriented polyethylene film (a commercial sandwich bag). For reference, the direction X is taken in the plane of the film perpendicular to the

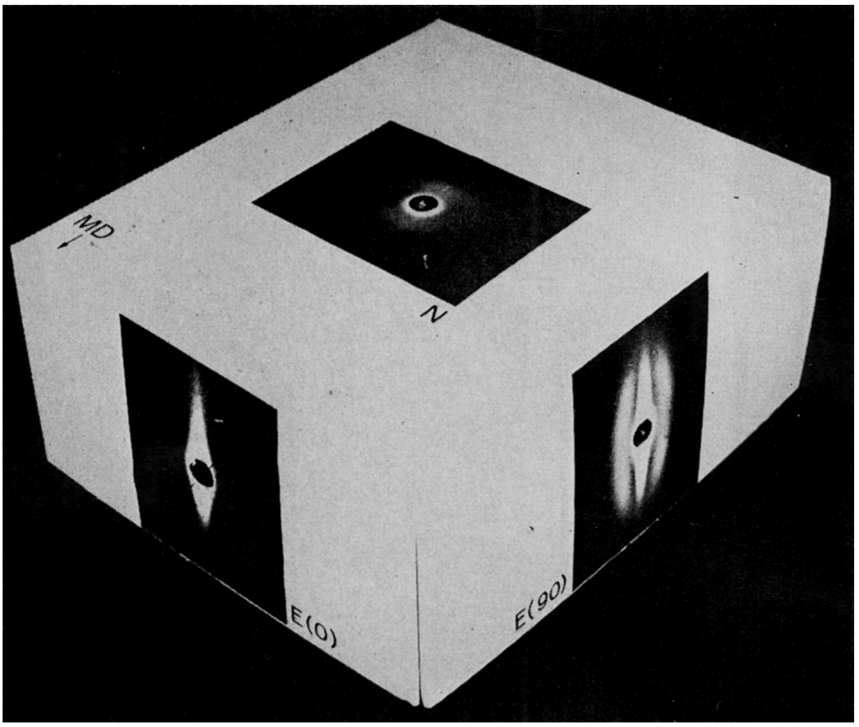

Fig. 6. Three-dimensional representation of the scattering observed for a reoriented (state IV via path 4) film prepared by postdeforming a state III film in the MD direction.

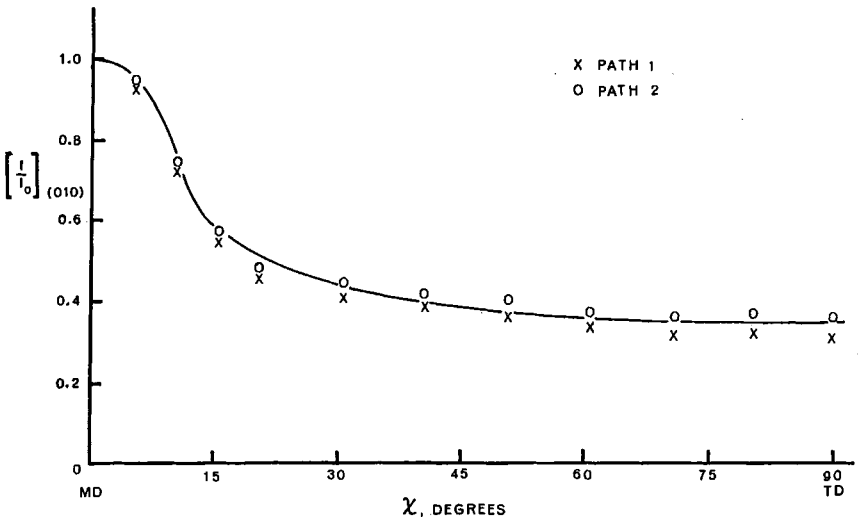

Fig. 7. Distribution of c-axes (crystallite orientation) for state II films prepared via paths 1 and 2. Densities: path 1, 1.379 g/cc; path 2, 1.393 g/cc.

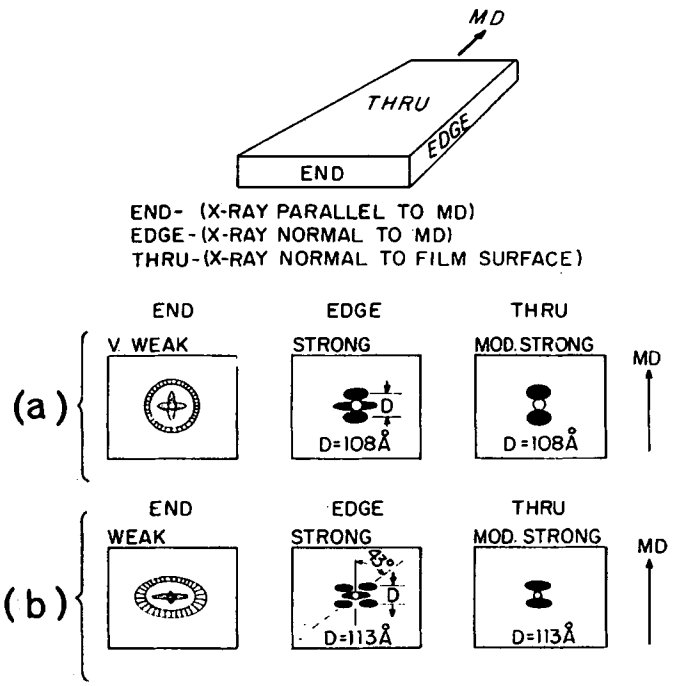

Fig. 8. Schematic representations of low-angle x-ray patterns for state II film at two levels of deformation: (a) 100% deformation; (b) 250% deformation.

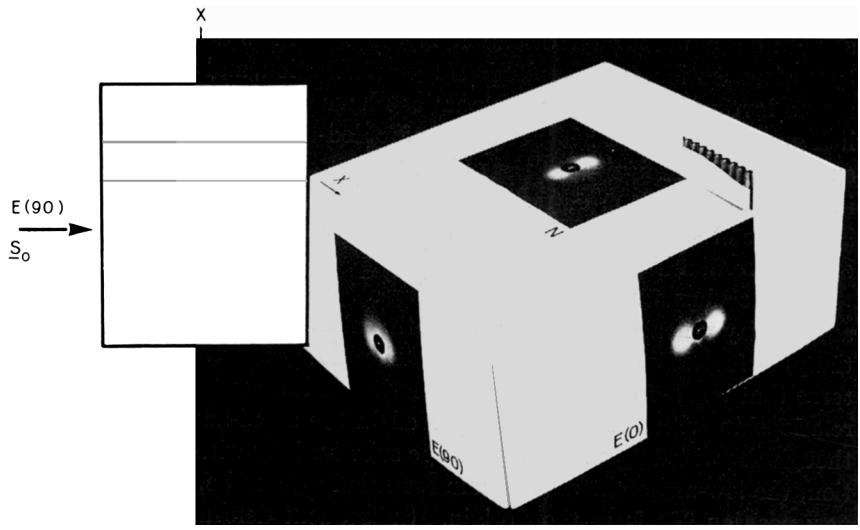

Fig. 9. Three-dimensional representation of the scattering observed from a polyethylene sandwich bag. The drawing shows how the direction X is defined relative to structural features of the bag.

open edge of the bag. A 156 Å long period is shown in the E(0) and N photographs. The E(90) view exhibits almost symmetrical scattering with weak maxima perpendicular to the film normal corresponding to a periodicity of 161 Å. This type of long period scattering is consistent with the model for a row-nucleated, folded-chain lamellar structure in which the lamellae (represented by a piece of corrugated cardboard in Fig. 9) are oriented parallel to the direction X. This morphology, thought to result from row nucleation, has been discussed in detail.[10,15,16]

A comparison of Figures 3 to 6 with Figure 9 and the discussion that follows in the next section demonstrate clearly that the structure of oriented PET film departs substantially from that thought to occur in oriented polyethylene.

DISCUSSION

The low-angle photographs are illustrative of the diversity of patterns obtainable with the same polymer system. Morphological interpretations must be consistent in explaining the scattering observed in all directions. Here, we compare the similarities and the differences that exist in the low-angle x-ray scattering from deformed structures of polyethylene and from PET. The differences observed in the low-angle scattering effects between fibers and films are also discussed. Low-angle scattering from films offers a minimum of one more degree of freedom than that obtained with oriented fibers because of the characteristic symmetries of each material.

Polyethylene

Keller and Machin[8] have demonstrated that several different types of structure are produced in oriented polyethylene films depending upon the type of nucleation, the magnitude of the deformation, and the thermal treatments involved. Plausible explanations have been presented for spherulitic growth as twisted helical ribbons of folded-chain lamellae growing from sporadic nucleation sites in the quiescent melt. Alternatively, nucleation in the sheared melt produces a dual fibrillar-lamellar crystalline structure. This type of stress-dependent morphology has now been shown to be present in several other polymer systems.[15,17]

Hendus[18] has studied the interrelationship between the wide- and low-angle x-ray diffraction patterns of both uniaxially and biaxially (sequentially) deformed polyethylene films. The changes in the wide-angle patterns that result from uniaxial deformation do not seem to have any clear relationship with the changes observed in the small-angle patterns. Although the wide-angle patterns change substantially with sample deformation, the low-angle patterns remain essentially the same, but rotate into a new position 90° from their origin. Subsequent deformation of the uniaxially drawn polyethylene films in a direction normal to the first shifts the molecular orientation toward the new direction of deformation. This causes the low-angle long-period spots to assume skewed positions. Hose-

mann[19] has induced similar skewing of the low-angle patterns by deforming the polyethylene structure in shear. This type of behavior has not been observed in the PET films discussed here. The biaxially drawn PET films were prepared using sequential and simultaneous methods of deformation.

Poly(ethylene Terephthalate) (PET)

A model for uniaxially deformed PET films was proposed by Statton and Godard[20] from a study of wide- and low-angle x-ray photographs. Their model consisted of parallel platelets stacked one upon another. Within each sheet, the individual crystallites of a crystalline-amorphous matrix were felt to be oriented in a chessboard array such that either a 2- or 4-point low-angle scattering pattern could be generated. The center streak was believed to be caused by the presence of microvoids or regions of low electron density.

Bonart[21] favors an extended chain structure for drawn PET fibers based upon a paracrystalline layer lattice in which the alternating crystalline and amorphous layers are inclined with respect to the fiber axis. This structure of PET is believed to result from the high chain flexibility and the low tendency to crystallize, which allows any folded chains to extend easily during deformation. The packing of this structure is again interpreted as a chessboard array of crystalline-amorphous regions to account for the quadrant scattering.

Yeh[22] has shown and Robertson[23] has proposed that "amorphous" PET is structured. Yeh believes the "amorphous" material is composed of 75 Å spherically shaped paracrystalline domains with the molecular chains passing from one domain to the next. Uniaxial deformation causes the ball-like domains to align in staggered rows at a substantial angle ($\sim$50°) to the direction of deformation. However, the *c*-axis orientation of the unit cell (obtained from the wide-angle patterns) is ordered essentially parallel to the direction of deformation. Electron-micrographic evidence shows an interball distance of 125 Å, in good agreement with the long-period data reported for uniaxially oriented PET films.[7,14] Biaxial deformation results in the development of block-like structures about 1000 Å long with their sides oriented 45° from the second direction of deformation. Yeh suggests that the 4-point low-angle x-ray pattern is related to a staggered arrangement of the spheres, whereas the 2-point pattern is a result of the balls being arranged in rows perpendicular to the stretch direction.

Fisher et al.[56] have described a clever method for comparing small-angle x-ray scattering patterns with the optical scattering patterns obtained from electron photomicrographs of the same polymer samples. They report excellent agreement of the intensity distributions and long period spacings from both techniques for drawn polyethylene and polyoxymethylene films. However, for the drawn PET samples they do not observe the expanded layers or lamellae usually associated with polyethylene but a texture described as "grainy." They believe this structure is indicative of a highly

disordered paracrystalline layer lattice. These results were obtained from observations of scattering made normal to the surfaces of the films.

Koenig and Hannon[24] argue that the annealing of oriented PET films results in structural relaxation and the creation of chain-folded lamellar domains. Two types of molecular folding are postulated: (1) regular folds which are measurable by infrared, and (2) irregular folds which are not observable. Subsequent post-deformation disrupts the irregularly folded domains. An annealing process then regenerates regular folding.

More recent studies[25] with oriented PET *fibers* annealed at constant length or constant tension suggest that the intensity of the low-angle long period spacing is a consequence of the number of regularly folded domains. The 2-point low-angle patterns were observed to change into 4-point quadrant patterns after thermal relaxation, in agreement with observations made with strain-relaxed polyethylene fibers.[26] These effects observed with PET fibers did not occur with the PET film structures reported here.

Two-phase[27] and paracrystalline[28] models have been suggested to explain the low-angle x-ray patterns observed for oriented polymers with relatively low crystallinity. These models have been used in conjunction with the concepts of lamellar unfolding and fragmentation to rationalize the existence of the observed 2- and 4-point scattering patterns. The deformation of the initially crystalline PET film (path 1) involves the concept of spherulite deformation, and ultimately the fragmentation of the chain-folded lamellar domains that presumably occur in the spherulite. Deformation from the glassy state (path 2) involves the rearrangement of a liquid-like structure which may have some regions of localized order. In all of the oriented PET film systems studied, the low-angle patterns we observed in the $E(\omega)$ directions had (1) the center streak close to the direct beam, and (2) the characteristic (2- or 4-point) long period scattering. We will focus our discussion on how these specific characteristics were found to change with the direction of viewing and the amount and type of sample deformation. Each will be considered in turn.

The Diffuse or Center Streak Scattering

Statton[5] has concluded for the diffuse scattering from fibers that:

1. The amount of diffuse scattering depends on the method of sample preparation.
2. Crystallinity is not the cause of, and has no relationship to, the diffuse scattering.
3. Scattering can be generated either by actual voids, as in cellulose, or by regions delineated by almost-periodic varying electron densities.

Submicroscopic voids (15–200 Å) have been shown to provide the best explanation for the diffuse scattering from cellulose fibers.[29] This has been confirmed quantitatively.[30] Voids in acid-leached glasses have also been identified by means of low-angle x-ray scattering.[31]

Fig. 10. Scanning electron micrograph of a fractured, biaxially oriented (path 3) film.

It is expected that voids should occur in polymeric systems regenerated from solution. However, in thermoplastic systems made from the melt, such as polyethylene, the nylons, and PET, it is not possible to decide from low-angle x-ray evidence alone whether voids, lamellar boundaries, or microcracks are the cause for the unique type of diffuse scattering called the center streak. The center streak scattering we observed was found to be independent of the amount of crystallinity and the type of crystallite orientation,[13] but dependent upon the temperature–tension history of the sample. These results are in substantial agreement with those reported for annealed PET fibers[25] for center streak scattering. However, our results suggest that the shape of the center streak in PET films is related to the differing electron densities of large platelet-shaped domains oriented essen-

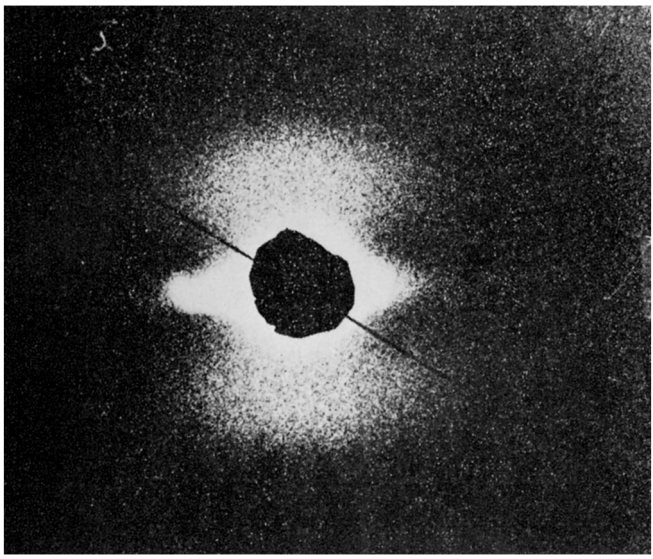

Fig. 11. An asymmetrical center streak in a path 3 film showing a semidetached spot.

tially parallel to the surface of the film. We do not know if the electron density differences occur between the lamellar sheets or from a distribution within the sheet itself, i.e., from the center to the surface boundary.

Platelets and Center Streak Scattering. The concept that oriented PET films consist of platelets or sheets has been demonstrated many times in the literature. For example, Statton and Godard's textural model[20] and Bonart's stacked platelet model[21] are based on microplatelets. In his etching experiments, Baker[32] has shown that micron-size platelets can be removed one at a time from the surface to the inside of the film and that the platelets removed decrease in thickness from the film surface inward. A scanning electron photomicrograph of a fractured path 3 PET film, Figure 10, demonstrates this macroplatelet structure quite convincingly. Optical microscopic observations of torn films reveals step-like fractures, and Yeh[22] has commented about delamination observed in the electron microscope. Heffelfinger and Burton[13] have reported that oriented PET films are highly uniplanar [e.g., most (100) crystallite planes[33] are oriented parallel to the film surface]. Wallach,[34] using light scattering, has demonstrated good correlations between these x-ray crystallite orientation distributions (a measure of the microstructure) with the light scattering patterns produced by the macrostructure. Such observations suggest that what is observed macroscopically progresses in general form into microstructural regions.

Hosemann and Bagchi,[35] Vainshtein,[36] and Guinier[37] describe the scattering expected from a structure composed of laminar platelets. This scattering can be expressed as the product of two $(\sin \zeta)/\zeta$ functions containing the dimensions of a rectangular aperture or lamina which would generate Fraunhofer diffraction. The zero*th*-order scattering maximum is spike

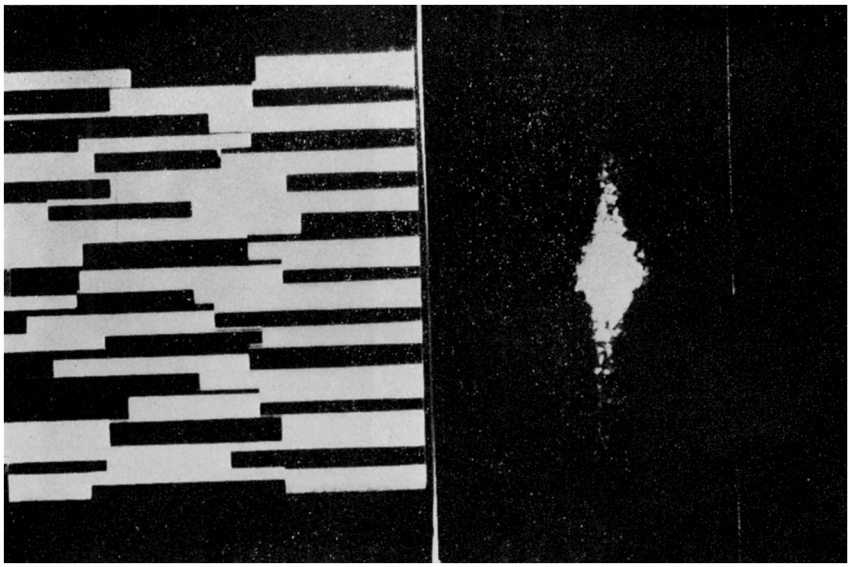

Fig. 12. (a) Mask representing collection of parallel laminae of statistically variable size, $\bar{l}/\bar{h} = 8$. (b) Optical diffraction from mask at (a).

shaped, with the long axis of the spike oriented perpendicular to the long axis of the aperture.

This same type of spike-shaped scattering has been observed with polycrystalline metals such as age-hardened aluminum–copper or aluminum–silver alloys. In these alloys, the scattering has been intepreted to result from structures produced by clusters of copper platelets[38] or platelets of Ag_2Al,[39] respectively. Mynard and Leak[39] reported that asymmetrical center streak scattering could be observed in these alloys depending on the position of the alloy sample with respect to the x-ray beam. Similar effects are sometimes observed in the center streak scattering of the films studied here, e.g., Figure 11 and Figure 18 at $\omega = 0$.

Model Structures. To aid our interpretation for the cause of the center-streak scattering, a series of optical masks[40] were prepared consisting of stacked laminar platelets with various average length-to-height ratios. A typical Fraunhofer scattering pattern from one of these masks ($\overline{l/h} = 8$), illustrated in Figure 12, shows a spike-shaped pattern very similar to that observed in the low-angle x-ray patterns. Mica and pyrolytic graphite are reasonable models for a stacked laminar system. These crystalline materials also exhibit center streak scattering, Figure 13, although of differing shapes and sizes.

Effect of Deformation and the Type of Crystallite Orientation. No center streak scattering is found in glassy or spherulitically crystalline PET films. However, the structure responsible for center streak scattering de-

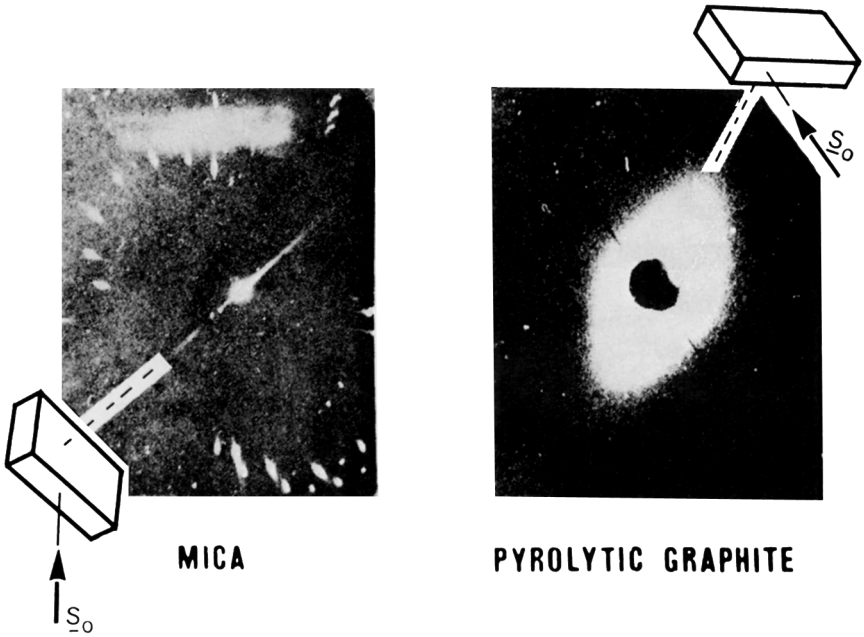

Fig. 13. Edge photographs of mica and pyrolytic graphite. Inserts show direction of x-ray beam (S_0) with respect to the geometry of the sheet.

velops at relatively low levels of film deformation (100%) when starting from the glassy state (path 2). We did not determine the deformation dependence for the path 1 films. Path 1 and 2 films, which have uniplanar-axial crystallite orientation, and path 3 films, with uniplanar orientation, all exhibit center streak scattering. The part 3 films (having a greater degree of uniplanar crystalline order[13]) generally have a much more pronounced spike-shaped pattern. The structure responsible for center streak scattering is essentially independent of the type, not amount, of orientation developed.

Crystallinity and Shrinkage. Thermal treatment (thermal crystallization and strain relaxation) was used to identify the influence of crystalline content and orientation on changes in the center streak scattering. Figure 14a shows the center streak developed in a path 2 or 3 PET film having low density (20% crystallinity). The laminar structure believed to be responsible for the center streak is thus formed independently of crystallinity. However, the order within the laminar structure of films with low crystallinity is not developed sufficiently to produce the long period scattering. In Figure 14b we illustrate the effect of thermal annealing (increasing crystallinity) under conditions of restraint for the path 2 and 3 films. The center streak is essentially unchanged, but the long period diffraction spots now make their appearance, indicating the development of ordered regions of smaller size (about 120 Å) than those responsible for the center streak. Progressing across Figure 14, pictures are shown representing the changes in

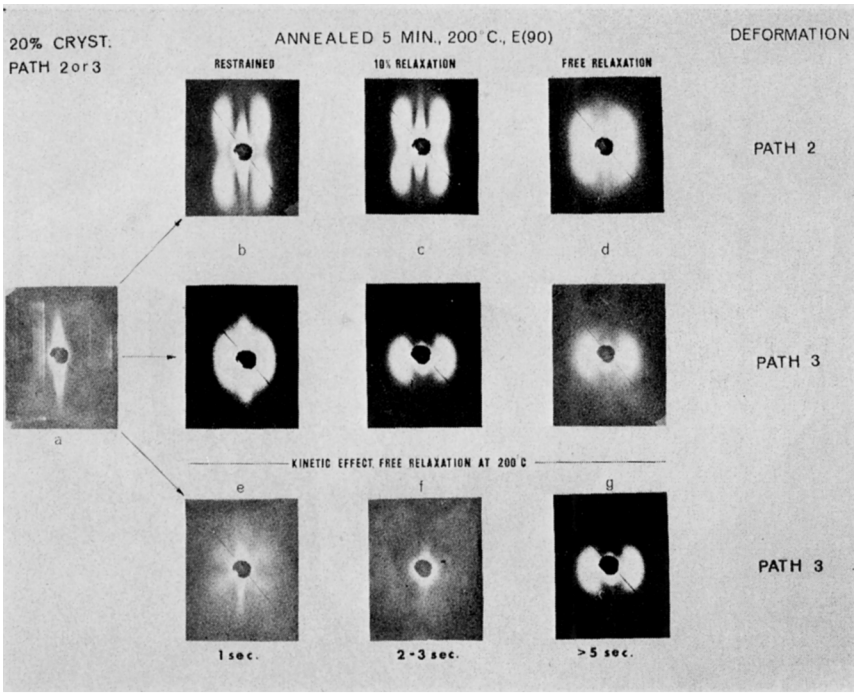

Fig. 14. Effect of heat treatments on the low-angle x-ray scattering from oriented PET films.

structural ordering produced by a 10% relaxation (shrinkage) (c), while (d) shows the effect of almost total relaxation (about 40% shrinkage in the planar directions). In each case the center streak is reduced in size, but the long period remains, although decreasing in magnitude.

Order-Disorder. Hosemann[19] has demonstrated the change in the center streak scattering that occurs when pressure is applied to cold-drawn polyethylene fibers. He proposes that pressure causes increased ordering of the structure for the following reasons: (1) the 2-point low-angle pattern of polyethylene develops into a 4-point pattern, and (2) the center streak decreases. Pressure is said to cause increased correlation between the layers and clusters of ultrafibrils. Thus he defines "voids" as the interstices between such clusters.

We suggest that just the opposite effect occurs in the strain-relaxed PET films studied here. Strain relaxation has been shown to cause structural disordering,[7] and we would thus expect less structural correlation after relaxation. In these oriented PET films the center streak scattering decreases in size, with apparent increases in structural disorder produced by relaxation.

The Size of Lamellar Sheets. If the center streak scattering originates from the way that large platelet domains are stacked, then it can be argued that the decrease in the size of the center streak is caused by an apparent

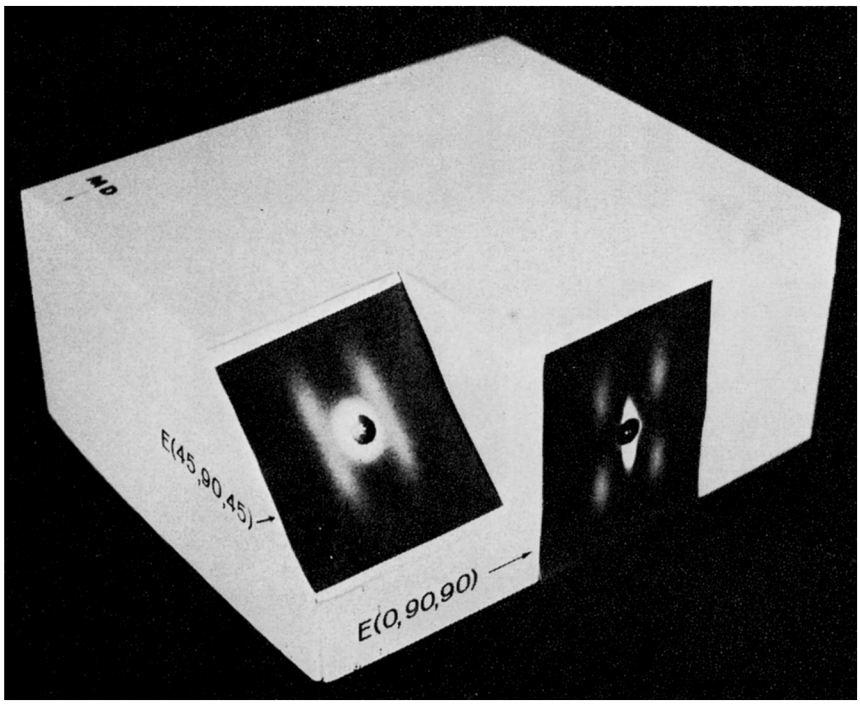

Fig. 15. Low-angle x-ray scattering from a path 2 film in positions E(0,90,90) and E(45,90,45).

increase in size as seen by the x-rays. This can occur from two sources: (a) physical thickening of the platelets, or (b) viewing them in a tilted position. The x-rays cannot discriminate between these alternatives. Changes in the size of the center streak are not a consequence of changes in relative intensity. X-Ray exposure times of 6, 24, and 160 hr yield the same results. In Figure 15 we demonstrate the severe foreshortening and broadening that occurs in the center streak when a film is viewed at the S_0 position E(45, 90, 45). This is merely a view of the scatter from a different direction. The foreshortening of the center streak in strain-relaxed structures therefore may be a consequence of either or both of the alternatives mentioned above.

Guinier[37] used an exponential approximation to the experimental curve of scattered intensities to determine the size of domains responsible for low-angle scattering. Hosemann has utilized this method to calculate a distribution of fibril sizes in polyethylene.[6] A Guinier-Hosemann analysis (described in the Appendix) was made of the intensity distribution [E(90) position] within the center streak of a path 2 film. The calculated thickness of the laminar domains varies from 290 Å to 3800 Å, with a length of 2000 Å to greater than 10,000 Å.

Theory predicts that the curve of scattered intensity versus angle should exhibit a series of minima for scattering produced from an individual plate-

let. The minima correspond to the zeros of a zero-order Bessel function of the first kind.[35,53] Normally, these minima in the scattering curve are not observed for systems containing multiple platelets, and the Guinier approximation has been assumed to apply. We have observed undulations in the scattering curves of the films reported here, when the angular dependent scattering was measured with a high-resolution Bonse-Hart small-angle scattering diffractometer. Recognizing the possible inadequacy of the theory to predict the scattering from systems of platelets, we were surprised to find that the positions of the minima observed corresponded to an average lamellar thickness of 2000 Å. This value agrees in magnitude with the results obtained by use of the Guinier approximation and from platelet sizes measured from scanning electron micrographs of fractured PET films, Figure 10. Our calculations are presented in the Appendix. A comparison of the results obtained from the Guinier-Hosemann treatment with those obtained from the observed minima in the scattering curve suggest that the center streak scattering is a consequence of platelet-shaped domains.

The Long Period Spacing

The structure responsible for the 2- or 4-point diffraction with a spacing of 100–150 Å is smaller than that responsible for the center streak scattering. These discrete patterns are dependent on the level of crystallinity and on the amount and type of crystallite orientation produced in the films studied here. In oriented PET films, the long period spacings usually reported are those obtained in the E(90) view, whereas in polyethylene films the long period reported is usually that observed in the N direction. Several investigators discuss a long period spacing for spherulitically crystalline PET films.[41,42] We have been unable to detect such long period spacings in the very weak diffuse scattering. The radially symmetric scattering decreases monotonically with angle, and no discrete intensity maxima have been observed.

Comments on Long Period Spacings. The long periods that occur with solution-grown polymer single crystals have been identified with the average fold length of the molecular chains by comparison with crystal thicknesses measured from electron micrographs. Annealing of these crystals results in an increase in the fold length and hence an increase in the long period spacing. The evidence is reasonably good that similar types of crystalline growth occur in polyethylene over the range of dilute solutions, concentrated solutions, and the quiescent melt.[43] In contrast to our understanding of the morphology of polymer single crystals, the structures responsible for the long period spacing in bulk-crystallized or highly oriented polymeric systems are not as well defined or understood.[44] Crystalline, bulk systems may yield either one or two discrete scattering maxima, depending on the conditions of sample preparation. The position of these maxima are not always in the ratio of 2:1, which would be expected from crystallographic diffraction orders arising from the same structural periodicity.[45,46]

One view[46] proposed to explain these nonintegral spacings is that the x-ray reflections in highly oriented systems result from a paracrystalline lattice such that the angular positions and the reflection intensities decrease with increasing lattice disorder. Two reflections would then be observed only in those systems for which the appropriate structure factors are large and the degree of disorder is low.

There is substantial evidence to justify the view that the long period diffraction is a consequence of the periodicity arising from folded-chain lamellae. Perhaps the best circumstantial evidence for this view is that long period diffraction is observed in solution-grown crystals[44] and in row-nucleated polymers,[8] both of which contain folded-chain lamellae, but not in extended-chain polyethylene crystals grown under hydrostatic pressure.[47]

The evidence for folding in highly deformed structures of PET is inconclusive. However, in unoriented crystalline PET, there is good evidence for chain folding. Keller has reported[12] that PET spherulites consist of helically twisted ribbons with the molecular chain axes oriented nearly perpendicular to the radial direction of the spherulite. This suggests that PET has the same type of spherulitic growth mechanism as that found in the spherulites of polymer systems known to develop folded-chain lamellae. Yamashita[48] has discussed the structure of PET crystals grown from solution by solvent evaporation. These lath-shaped crystals were imperfect, but the diffraction patterns indicated that the molecular chains were oriented 25°–35° from the normal to the basal (fold) planes. For the molecular weights he used, the chains could fit only by folding.

It is possible to demonstrate with molecular models that PET will fold sharply upon itself over one repeat unit. Long period spacings in PET are found to increase with crystallization temperature in the same way as those reported for polyethylene.[41] Koenig and Hannon[24] have assigned the 988 cm^{-1} infrared band of PET to a fold conformation. The arguments they present would indicate the likelihood of folded domains in oriented PET films resulting from annealing, or strain relaxation, or both. One unreconciled point is the presence of the 988 cm^{-1} infrared band in the trimer which cannot fold.[49,50] Nevertheless, the possibility of folded domains cannot be dismissed as the likely source of the long period diffraction in oriented PET films.

Two concepts are troublesome in the broad morphological interpretation of the films reported here: (1) the origin of the 4-point quadrant diffraction, and (2) the spatial orientation of folded domains (if they exist) which would produce the observed discrete scattering.

Interpretations of the cause for the long period diffraction in PET films must be consistent with the orientation of the molecular chains and with the relaxation effects observed.

The Effect of Deformation on the Long Period. Figures 14e to 14g illustrate the development of the long period diffraction of a path 3 film by unrestrained thermal annealing in 200°C air for short times. Several phenomena are observed: (1) A transient X-shaped scattering makes its

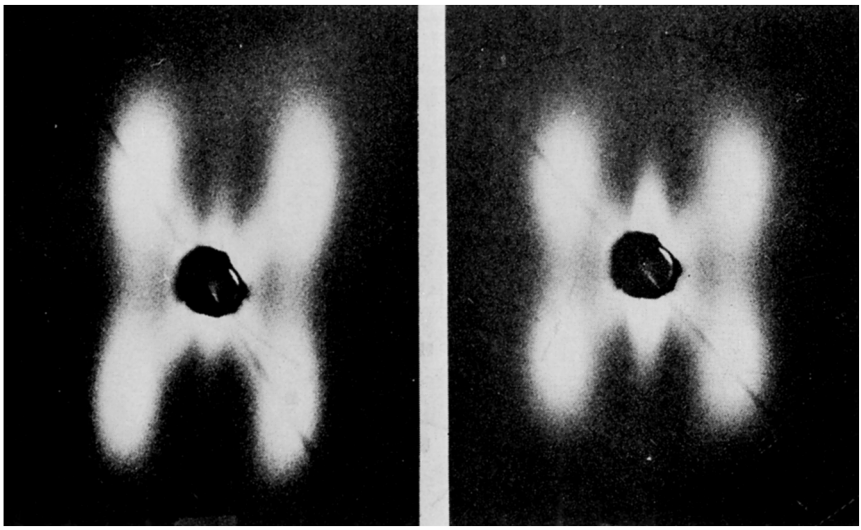

(a) (b)

Fig. 16. Effect of 10% relaxation during heat treatment at 200°C on the E(90) long period scattering of a path 2 film initially oriented to 300% elongation. For this figure only, the specimen-to-film distance is 32.0 cm: (a) restrained during heat treatment for 5 min at 200°C; (b) 10% relaxation allowed during heat treatment at 200°C for 5 min.

appearance first, within about 1 sec (e), (2) this scattering disappears in 2–3 sec (f) and is ultimately replaced by the 2-point long period spots (g). Within this period of time, the crystallinity in the film has increased from 20% to 41%. The transient low-angle x-ray scattering pattern looks like the $(H + V)_v$ optical scattering patterns reported from the macrostructures of PET.[34] This effect may be a consequence of the rapid rearrangement of the ball-like domains into new positions, as discussed by Yeh.[22]

The X-shaped scattering persists, however, in the path 1 and path 2 films. This is particularly apparent in the 32-cm diffraction pictures of Figure 16. Here, the 4-point spots are connected through the beam stop with the same type of pattern observed in Figure 14e. Therefore, the structure that is produced in the path 1 and path 2 films is not destroyed as a consequence of annealing. The appearance of the transient structure in the path 3 films during annealing suggests that some memory of its previous state may have been retained.

Figure 8 illustrates the changes in the type of long period pattern developed by path 2 films as the level of sample deformation is increased. The 4-point pattern begins to form only at film deformations exceeding 200–250%. Below this level, a 2-point pattern is formed. The long period and the equatorial spacing of the quadrant diffraction change as a function of deformation, as shown in Figure 17. The registry of diffracting domains (the long period), parallel to the direction of deformation, is relatively insensitive to the amount of deformation until quite high levels of strain (400%)

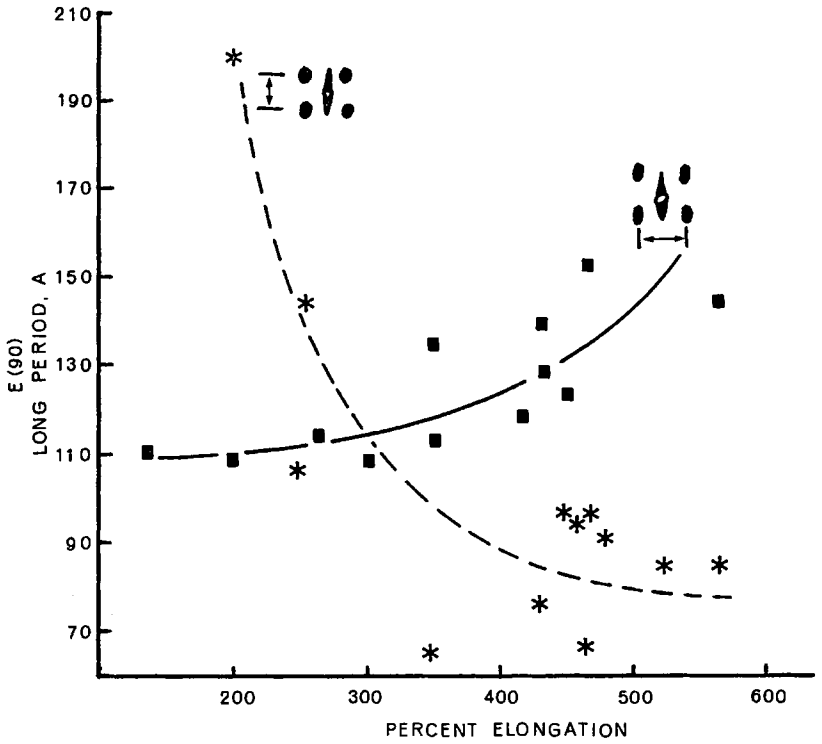

Fig. 17. Changes in long period spacings as a function of percent elongation. The diagram shown with each curve indicates the dimension in reciprocal space used to calculate the corresponding long period.

are involved. Alternatively, the registry of domains in a direction normal to the film surface begins to decrease quickly at low deformations, indicating a greater degree of structural packing in the thickness direction. The rapid change that occurs at 250% elongation coincides with the development of substantial uniplanar-axial crystalline orientation as discussed previously.[13] The domains responsible for the E(90) scattering that produce the quadrant pattern are likely arranged in ordered diagonal arrays. Whatever their macromorphology, the molecular chain axes are aligned primarily in the direction of deformation.

The long period is a function of the level of crystallinity, but the spacing obtained is proportional to the amount of strain in the structure. Strain relaxation (shrinkage), Figure 14, decreases the long period spacing.[7] This is shown quite clearly in Figure 16, with a path 2 film in which 0 or 10% shrinkage was permitted during heat treatment at 200°C for 5 min. The long period has decreased from 125 Å to 112 Å, while the spacing parallel to the film normal has increased from 94 Å to 112 Å.

Differences in the Scattering Between Fibers and Films. Several observations reported for the low-angle x-ray scattering from drawn PET fibers

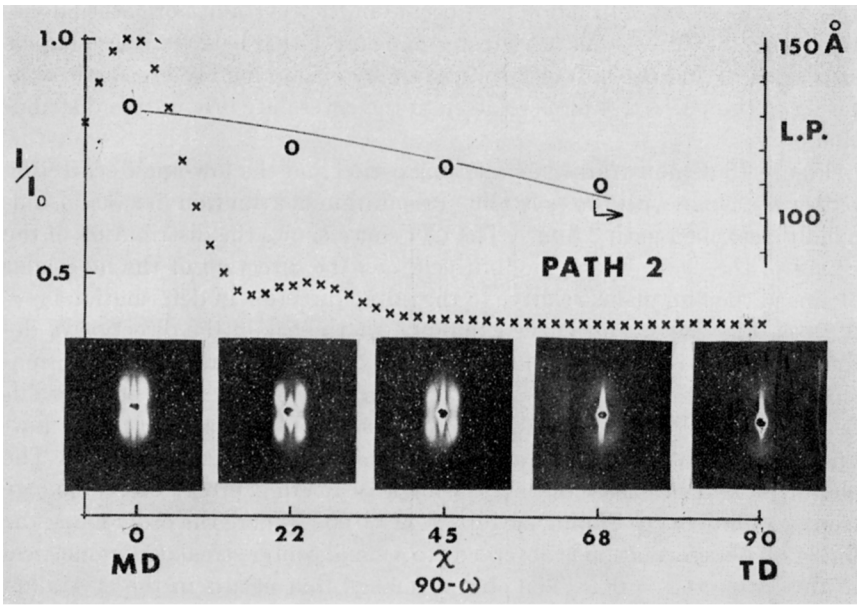

Fig. 18. Long period and distribution of the *c*-axis as a function of angle for a path 2 film.

were found to be different from those observed with the films studied here. For example, strain relaxation with fibers causes the 2-point pattern to change to a 4-point pattern.[25,26] Beresford and Beven[51] have observed that the application of tension to drawn nylon fibers causes the scattering to change from a 4-point to a 2-point pattern. We mentioned earlier the differences observed in the center streak when a fiber is subjected to radial compression. Morphological interpretations have been proposed for fibers on the basis of this type of behavior.

The series of pictures in Figures 14b to 14d illustrate that the strain relaxation of a uniaxially deformed film causes the 4-point (quadrant) scattering to degenerate to the 2-point (equatorial) pattern. We have discussed above the change from 2- to 4-point diffraction with increased strain in PET film. Clearly, structural interpretations based on fiber geometry are not necessarily valid for films.

The path 3 films exhibit only broad 2-point diffraction patterns, indicating that the three-dimensional registry that produces quadrant diffraction has been reorganized. In contrast to polyethylene, no rotation of the diffraction spots has occurred by deforming the structure in the second direction. The path 4 films produce a type of quadrant diffraction, but again, with no rotational change in the position of the spots. Consequently, the structural rearrangements that occur from the biaxial deformation (sequential or simultaneous) of PET are different from those observed with polyethylene.

Coupling Between the Micro- and Macrostructures. The domains responsible for the long period diffraction (~115 Å) are larger than those

responsible for the diffraction that occurs in the crystallite orientation distributions (~10 Å). We have tested the correlation between these larger-size domains and the unit cell orientation by examining the low-angle scattering of the paths 2–4 films relative to the crystallite orientation distribution curves.

Figure 18 demonstrates how the long period and the low-angle scattering patterns change with the crystallite orientation distribution in a 300% uniaxially deformed path 2 film. The (X) curve shows the distribution of the c-axes of the crystallographic unit cell, i.e., the direction of the molecular chains in the film plane, relative to the initial direction of deformation ($\chi = 0°$) (see Fig. 2b). This curve exhibits a sharp peak in the direction of deformation and decreases quickly (within 22°) from the direction of deformation. The peak that appears at 22° is an interference from another diffracting plane.[13] Below the curve of crystallite orientation are the low-angle x-ray photographs taken as a function of the angle ($90° - \omega$). The character and intensity of the low-angle scattering progressively change from a well-defined 4-point pattern at $\omega = 90°$ (where the order along the direction of deformation is observed) to a small center streak (asymmetrical in this case) at $\omega = 0°$. The abrupt change that occurs in the crystallite orientation distribution is not mirrored in the curve of the long period spacings. The long period decreases smoothly from 130 Å at $\omega = 90°$ to 110 Å at $\omega = 68°$, beyond which it is no longer visible.

Figure 19 has the same type of information for a path 3 film. A "balanced" biaxially deformed film has a uniform c-axis orientation distribution, i.e., there is no preferred direction of molecular orientation within the plane

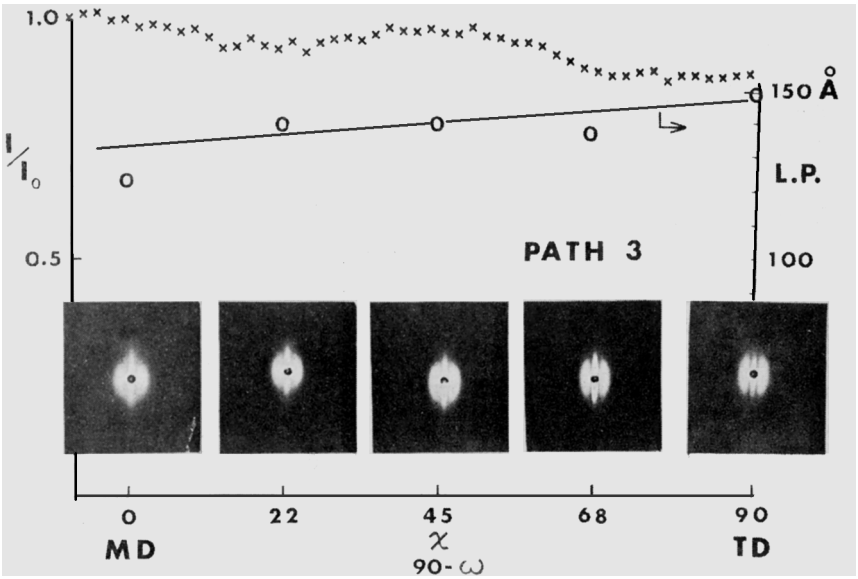

Fig. 19. Long period and distribution of the c-axis as a function of angle for a path 3 film.

of the film. The low angle scattering patterns are now all typical 2-point, while the long periods remain essentially the same, averaging 132 Å in the sample shown. The quadrant scattering is partially regenerated by further deformation of the path 3 films. This can be seen in Figure 20, which shows the reorientation and the angular dependence of the scattering for a path 4 film. Here the E(90) scattering appears to consist of a combination of 4- and 2-point diagrams yielding crescent-shaped patterns. The distribution curve for the *c*-axis shows a preferential alignment toward the direction of final deformation, but once again the decrease in the long period spacing with angle changes more gradually than the crystallite orientation. This evidence suggests that the structure responsible for the

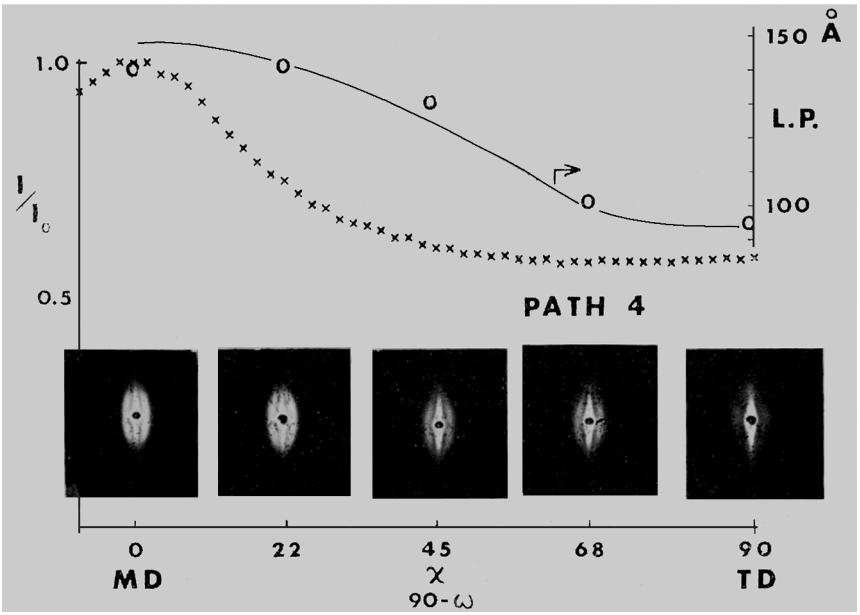

Fig. 20. Long period and distribution of the *c*-axis as a function of angle for a path 4 film.

crystallite orientation diffraction is not closely coupled to the structure responsible for the long period scattering.

The Direction of Observation. The appearance of the 4-point pattern in the path 2 films depends on the direction of viewing. In Figure 15, we demonstrate the change in character of the 4-point pattern as S_0 is moved toward the film normal. The 4-point pattern coalesces and ultimately yields only a 2-point pattern (N view of Fig. 4). As the direction of viewing is changed between E(0, 90, 90) and E(90, 90, 0), the character of the 4-point pattern assumes, at intermediate positions, a shape similar to the E(90) view of the path 4 film, Figure 6. Consequently, both the spacing and the type of pattern observed in oriented films are highly dependent upon the geometry and the direction with which the system is viewed.

We offer the following as one way of thinking about the structure of the polymer films reported here. At least three types of organization of structural domains are involved. The smallest is measured by wide-angle x-ray diffraction and involves the distribution of crystallite unit cell planes and axes (5–15 Å) relative to a frame of reference within the film.[7,13] Next in size are the domains (ordered or disordered) that produce discrete low-angle x-ray diffraction effects having a periodicity of 100–150 Å. We are uncertain of the morphology responsible for this periodicity. The largest domains observable by x-ray scattering are the platelet structures believed to cause the diffuse center streak scattering about the beam stop.

The type of low-angle x-ray pattern obtained is dependent upon the method of sample preparation and upon the direction of observation. We suggest that the shape and intensity of the discrete long period-type diffractions are caused by combinations of large structural elements moving as units in shear parallel to the direction of strain. Consequently, we believe that various layers within the film are viewed in different directions depending on the deformation history of the sample. Fixed within these larger domains are scattering centers arranged to yield 4-point quadrant diffraction effects only when viewed in the proper direction. The intensity of the long period diffraction spots decreases in the order of path $2 > 3 > 4$.

It has been proposed that the long period intensity is proportional to the number of fold domains in fibers.[52,25] Few regular folds are reported to exist in highly oriented PET film.[24] We have been unable to devise a satisfactory model for highly oriented PET films containing primarily folded-chain crystalline lamellae that is consistent with: (a) the crystalline orientation distributions; (b) the orientation distributions measured by refractive index and infrared methods; (c) the mechanical properties measured in-plane and in the thickness direction; (d) the shrinkage and expansion characteristics that exist in-plane, and out-of-plane as a function of temperature. Consequently, we are unconvinced that the morphology responsible for the long period diffraction in highly oriented PET films consists of folded-chain lamellar domains.

In summary, we have attempted to demonstrate, with one polymer system deformed in various ways, the variety of low-angle scattering patterns that can be generated. Within this system we have reproduced almost all the types of patterns reported for polymers of various kinds. Substantial differences have been demonstrated between the scattering patterns of polyethylene and PET upon deformation. Some similarities have also been noted. It is suggested that interpretations of fiber morphology based on low-angle x-ray scattering effects may not be applicable to films. Emphasis has been given to the effect of the observation direction on the patterns observed. A platelet structure for oriented PET has been proposed to explain center streak scattering.

The similarity of the structures produced by deforming either the precursor glass or the spherulite indicates that a particular polymer has a preferred way of aggregating under stress. It is significant that the same struc-

ture (state II) is obtained in both cases. The implication is that the same final structure can be obtained independent of the deformation and crystallization paths used.

APPENDIX

The Size of Domains That Produce Center Streak Scattering

The inverse dependence of domain size on the scattering angle is useful for determining the size and shape of polymer macrostructural regions. Scattering intensities near the direct beam decrease rapidly with angle such that the shape and intensity of the initial part of the scattering curve can be approximated by an exponential function (Guinier[37]). Hosemann (cf. ref. 6) has used this approximation for resolving the scattering curve of polyethylene structures into Gaussian components. In this way, a distribution of domain sizes is calculated. We will call this method I.

The scattering observed from an isolated spherical domain is described by the major features of the first-order spherical Bessel function $j_1(2\zeta)$, the Fourier transform of a sphere, ($\zeta = Hr/2$, where r is the radius and H is defined below). If scattering occurs from a collection of objects, then interparticle interference becomes important and the details of the scattered radiation field at very low angles are distorted relative to that observed with the isolated particle. In spite of this degradation, the essential features of the $j_1(2\zeta)$ function for spherical domains are observed beyond the first two or three minima in the scattering from thick dried films of latex spheres.[54,55]

An isolated platelet-shaped object has a Fourier transform described by a zero-order spherical Bessel function $j_0(\zeta)$. Undulations occur in the scattering curve from individual platelet-shaped domains which correspond to the periodic minima in the (sin ζ)/ζ function. Periodic minima have not been reported for polymeric fibers or films believed to contain collections of platelet-shaped domains. If observable minima are present, then the average size of the domains responsible for the scattering can be calculated independent of the Guinier approximation. We were able to do this (method II), and we compare here the results of the domain size calculations obtained with and without the exponential approximation. The center streak scattering from a path 2 film in the E(90) position was used.

EXPERIMENTAL

High-resolution x-ray intensity measurements were made with a Bonse-Hart diffractometer[54] (CuKα radiation) at intervals of 20 sec of arc from a 2θ = 20 sec to 0.3° along the major axis and at 2-sec intervals to 2.5 min along the minor axis of the center streak. The scattered intensity was observed by a scintillation counter without pulse height analysis Intensity and scaling times were such that, after averaging the seven independent scans, each measured intensity at a given angular increment had a precision not exceeding 4% of its value. The intensity curve observed was not desmeared.

Method I (Guinier and Hosemann)

The intensity versus angle data were treated as shown in Figures 21 to 23:

1. To obtain the appropriate function for calculation, the logarithm of the average observed intensity versus angle was tabulated. An interpolation was performed to yield a table of ln I versus H, where $H = 4\pi \sin\theta/\lambda$ (θ = scattering angle/2 and λ = 1.5418 Å, the wavelength of CuKα radiation). The interpolation procedure made use of a quadratic polynomial to fit five successive data points (nos. 1–5), and the interpolated points were generated from the two center regions, i.e., between points 2 and 3 and 3 and 4. A new polynomial was then fit to points 3–7 and the procedure repeated over the entire curve. This process produced the curve shown in Figure 21.

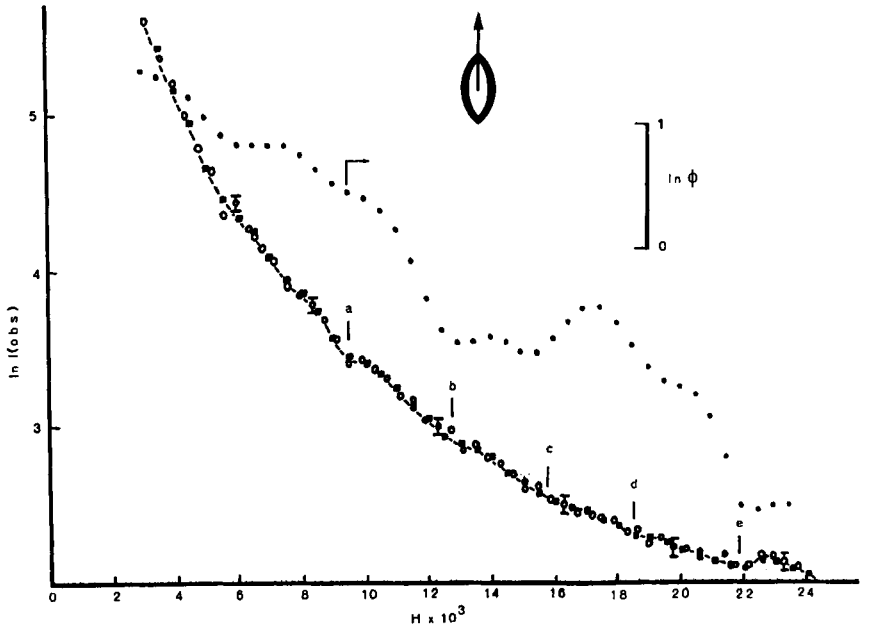

Fig. 21. Plot of $ln\ I_{obs}$ vs. H along the major axis of the center streak (path 2 film): (O) observed data; (■) interpolated data; (●) Bessel function summation resulting from the Guinier-Hosemann decomposition; 4% limit of error shown by vertical bars.

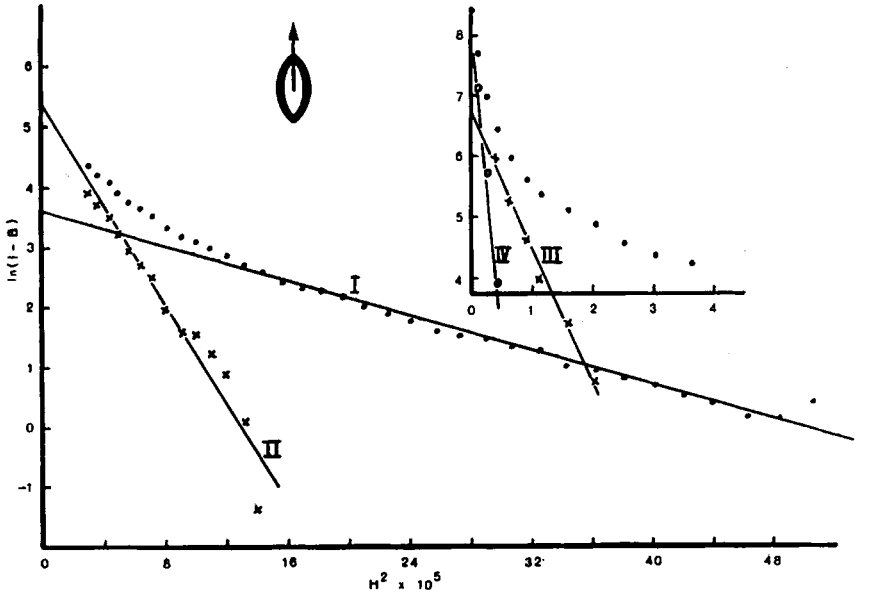

Fig. 22. Guinier-Hosemann decomposition of the center streak scattering along the major axis (path 2 film): (●) observed data; (×,O) data with components subtracted.

TABLE A-I

Method I—Results of the Guinier-Hosemann Decomposition of Observed Scattering Curves

Direction	Component	H_{min}, Å^{-1}	Number of points fit	$I(0) - B$	R_D, Å	t, Å	t_i/t_1	Abundance,[a] %
Major (thickness)	I	0.95×10^{-2}	25	37.0	84.3	292	1.00	28
	II	0.55×10^{-2}	14	209	203	703	2.41	27
	III	0.2×10^{-2}	6	875	473	1,640	5.62	21
	IV	0.5×10^{-3}	3	5230	1100	3,810	13.0	24
					Weighted av. =	1,530		
Minor (length)	I	0.145×10^{-2}	38	44.7	593	2,050	1.00	23
	II	0.8×10^{-3}	15	418	1520	5,260	2.56	32
	III	0.4×10^{-3}	9	2240	2980	10,300	5.02	45
					Weighted av. =	6,787		

[a] Relative abundance calculated as $(I(0) - B)/(t_i/t_1)^2$.

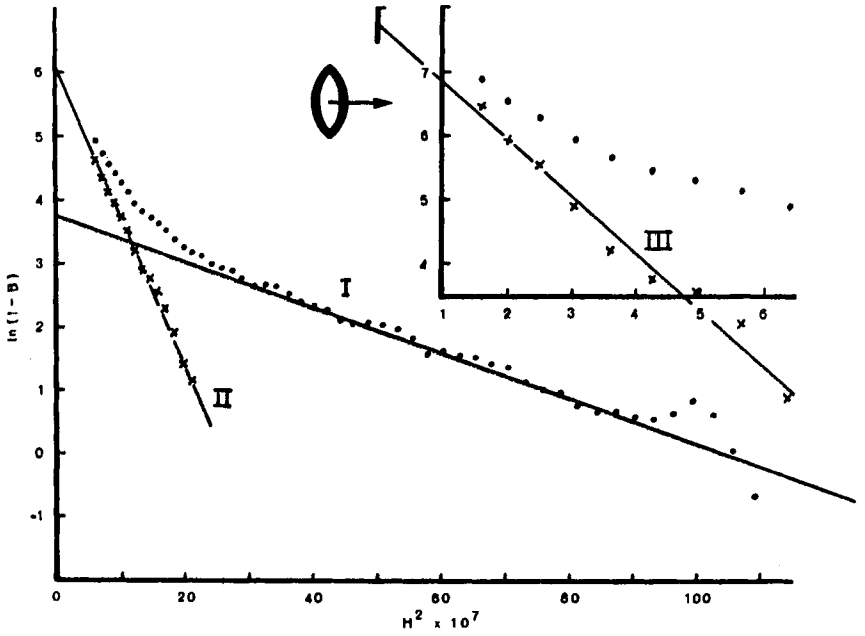

Fig. 23. Guinier-Hosemann decomposition of the center streak scattering along the minor axis (path 2 film): (●) observed data; (×) data with components subtracted.

2. The empirical Porod equation $I = A/H^4 + B$ was used with the interpolated data to evaluate the constant B, which represents the angularly independent component of the observed scattering.

3. A plot of ln $(I - B)$ versus H^2 was developed using the Guinier approximation,

$$(I - B) = [I(0) - B] \exp [-R_D^2 H^2],$$

which relates the angularly dependent portion of the data to the radius of gyration, R_D, of oriented scattering domains. If scattering arises from domains of a single size, then the Guinier plot is a straight line. For the center streak scattering from the path 2 film, substantial curvature exists at low H values, suggesting a broad size distribution.

4. The curve was decomposed into several straight line segments (Figs. 22 and 23), as follows: (a) At high H values, where the scattering curve is relatively linear, a least-squares straight line could be fitted easily. The slope of this line is R_{D1}^2 (the radius of gyration squared) of the first Gaussian component. (b) Using the slope and intercept of this line, values of I_{calc} were computed and subtracted from I_{obs}. This yielded a new set of intensity data from which R_{D1} is missing. Thus, the procedure can be repeated to yield $R_{D2} \cdots R_{Dn}$.

5. The thickness of each lamellar unit is calculated as $\sqrt{12}$ times the value of R_D, where the $\sqrt{12}$ is the numerical factor relating the radius of gyration of a plate to its thickness. Table A-I lists the size data obtained by decomposing the scattering curve in this manner.

Method II (From Scattering Theory)

Visual inspection of the curve ln I_{obs} versus H along the major axis of the center streak indicated periodic minima at five H values, as shown in Figure 21. A zero-order spherical Bessel function, $j_0(\zeta)$ for scattering from a plate has the argument $Ht/2$, where t is the

TABLE A-II
Method II—Thicknesses Based on Position of Minima in Observed Scattering Curve Along Major Axis Direction[a]

Direction	Minima	$Ht/2$	H_{obs}, Å^{-1}	t, Å
Major	a	3π	9.4×10^{-3}	1990
(thickness)	b	4π	12.8×10^{-3}	1970
	c	5π	15.8×10^{-3}	2000
	d	6π	18.5×10^{-3}	2040
	e	7π	21.8×10^{-3}	2020
				avg. = 2000

[a] Relative agreement, methods II/I = 2000 Å/1530 Å = 1.3.

thickness and H has been defined previously. The average separation between the minima was about 3×10^{-3} units of H, indicating that the first observed minima at 9.4×10^{-3} Å^{-1} was the third zero of the Bessel function. The function becomes zero at values of the argument $n\pi$, where n is an integer. Substituting the values of H at the minima into the argument of the function yielded the thickness values given in Table A-II for each minima. The average size of the domains in the thickness direction is about 2000 Å.

The error in the intensity measurements was 4%. The minima observed are within the confines of the measurement error, as shown in Figure 21. Nevertheless, we believe it unlikely that errors in the scattering measurements, influenced by chance alone, would result in such periodic minima.

Minima are also present in the scattering curve along the minor axis, but it was not possible to use these to obtain an average size distribution (Fig. 24). The minima observed in this direction are aperiodic. This is likely a consequence of the existence of

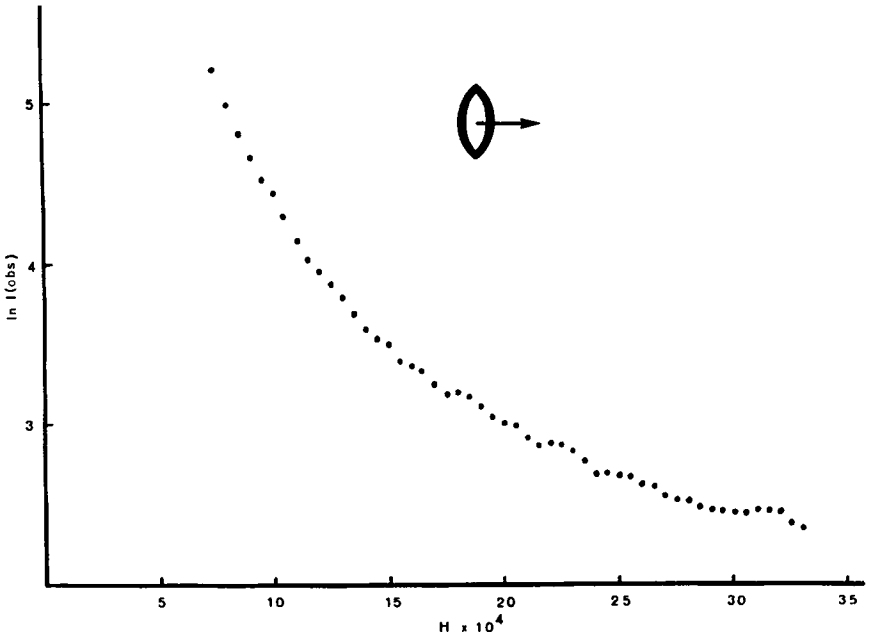

Fig. 24. Plot of $ln\ I_{obs}$ vs. H along the minor axis of the center streak (path 2 film). The value of $ln\ I$ is 13.8 at the origin.

very large domains which would produce a high frequency of superimposed minima beyond the resolution limit of the data. To support this point of view, the Guinier-Hosemann analysis indicates that the size distribution is skewed toward lengths in excess of 10,000 Å (Table A-I).

CONCLUSION

The results of the Guinier-Hosemann treatment (method I) were compared with those of method II by generating a Bessel function sum from the derived thicknesses and the relative abundances, e.g.,

$$\phi = \left[\sum_{i=1}^{n} \alpha_i j_0(Ht_i/2)\right]^2 \quad \text{where } \alpha_i = \frac{\%\text{ abundance}}{100}.$$

The function that results from treatment of the major axis data of Table A-I, shown in Figure 21, has periodic minima in reasonable agreement with those observed experimentally. A similar analysis along the minor axis yielded a function containing a high frequency of minima that had little relation to the observed scattering curve.

On the basis of this evidence, we believe that the treatment described by method I, i.e., resolving the measured scattering curve into its Gaussian components, yields results representative of center streak scattering from large platelet-shaped domains.

References

1. R. Hosemann, in *Small-Angle X-Ray Scattering*, H. Brumberger, Ed., Gordon and Breach, New York, 1967, p. 169.
2. P. Predecki and W. O. Stratton, in *Small Angle X-Ray Scattering*, Brumberger, H., Ed., Gordon and Breach, New York, 1967, p. 131.
3. W. O. Statton, *J. Polym. Sci.*, **41**, 143 (1959).
4. R. Bonart and R. Hosemann, *Kolloid-Z. Z. Polym.*, **186**, 16 (1962).
5. W. O. Statton, in *Polymer Reviews*, Vol. 6, B. Ke, Ed., Wiley, New York, 1964.
6. L. E. Alexander, *X-Ray Diffraction Methods in Polymer Science*, Wiley-Interscience, New York, 1969.
7. C. J. Heffelfinger and P. G. Schmidt, *J. Appl. Polym. Sci.*, **9**, 2661 (1965).
8. A. Keller and M. Machin, *J. Macromol. Sci., (Phys.)*, **B1(1)**, 41 (1967).
9. E. S. Clark, *SPE J.*, **23**, 46 (1967).
10. J. J. Dietl, *Kunststoffe*, **59**, 515 (1969).
11. W. H. Cobbs, Jr. and R. L. Burton, *J. Polym. Sci.*, **10**, 275 (1953); K. G. Mayhan, W. J. James, and W. Bosch, *J. Appl. Polym. Sci.*, **9**, 3605 (1965).
12. A. Keller, *J. Polym. Sci.*, **17**, 291, 351 (1955); Keller, A. and Waring, J. R. S., *J. Polym. Sci.*, **17**, 447 (1955).
13. C. J. Heffelfinger and R. L. Burton, *J. Polym. Sci.*, **47**, 289 (1960).
14. G. Yeh, *J. Macromol. Phys.*, **B1**, 251 (1967).
15. E. S. Clark and C. A. Garber, The Effect of Industrial Processing on the Morphology of Crystalline Polymers, Presented at AIChE Meeting, Atlanta, Georgia, February 1970.
16. K. Kobayashi and T. Nagasawa, *J. Polym. Sci. C*, **15**, 163(1965).
17. E. H. Andrews, through personal communication from W. O. Statton.
18. H. Hendus, *Kolloid-Z., Z. Polym.*, **165**, 32 (1959).
19. R. Hosemann, *Polymer*, **3**, 349 (1962).
20. W. O. Statton and G. Godard, *J. Appl. Phys.*, **28**, 1111 (1957).
21. R. Bonart, *Kolloid-Z. Z. Polym.*, **199**, 136 (1964).
22. G. S. Y. Yeh, Doctoral Dissertation, Case Institute of Technology, November 1966.
23. R. E. Robertson, *J. Phys. Chem.*, **69**, 1575 (1965).
24. J. L. Koenig and M. J. Hannon, *J. Macromol. Sci. (Phys.)*, **B1(1)**, 119 (1967).

25. W. O. Statton, Presented at American Physical Society, Los Angeles, December 29, 1969.
26. B. Belbeoch and A. Guinier, *Makromol. Chem.*, **31**, 1 (1959).
27. W. O. Statton, *J. Polym. Sci.*, **41**, 143 (1959).
28. R. Hosemann, *J. Appl. Phys.*, **34**, 25 (1963).
29. W. O. Statton, *J. Polym. Sci.*, **22**, 385 (1956).
30. P. H. Hermans, A. Weidinger, and D. Heinkens, Presented at the First Cellulose Conference at the Cellulose Rearch Institute, Syracuse, New York, April 24, 1958.
31. H. Brumberger and P. Debye, *J. Phys. Chem.*, **61**, 1623 (1957).
32. W. P. Baker, *J. Polym. Sci.*, **57**, 993 (1962).
33. R. deP. Daubeny, C. W. Bunn, and C. J. Brown, *Proc. Roy. Soc.* (London), **A226**, 531 (1954).
34. M. L. Wallach, *J. Polym. Sci.*, **C13**, 69 (1966).
35. R. Hosemann and S. N. Bagchi, *Direct Analysis of Diffraction by Matter*, North Holland, Amsterdam, 1962, Chap. 12.
36. B. K. Vainshtein, *Diffraction of X-Rays by Chain-Like Molecules*, Elsevier, New York, 1966.
37. A. Guinier and G. Fournet, *Small-Angle Scattering of X-Rays*, Wiley, New York, 1955.
38. A. Guinier, *Physics Today*, **22**, 25 (November 1969).
39. B. A. Mynard and G. M. Leak, *J. Appl. Crystallogr.*, **2**, 101 (1969).
40. C. A. Taylor and H. Lipson, *Optical Transforms*, G. Bell and Sons, London, 1964.
41. K. L. O'Leary and P. H. Geil, *J. Macromol. Sci. (Phys.)*, **B1**(1), 147 (1967).
42. H. G. Zachman and G. F. Schmidt, *Makromol. Chem.*, **52**, 23 (1962).
43. A. Keller, *Polymer*, **3**, 393 (1962).
44. P. H. Geil, *Polymer Single Crystals*, Interscience, New York, 1960.
45. P. H. Geil, *J. Polym. Sci.*, **C13**, 149 (1966).
46. P. H. Lindenmeyer and R. Hosemann, *J. Appl. Phys.*, **34**, 42 (1963).
47. P. H. Geil, F. R. Anderson, B. Wunderlich, and T. Arakawa, *J. Polym. Sci. A*, **2**, 3707 (1964).
48. Y. Yamashita, *J. Polym. Sci. A*, **3**, 81 (1965).
49. E. Ito and S. Okajima, *Polymer Letters*, **7**, 483 (1969).
50. I. Goodman and B. F. Nesbitt, *J. Polym. Sci.*, **48**, 423 (1960).
51. D. R. Beresford and H. Bevan, *Polymer*, **5**, 247(1964).
52. P. F. Dismore and W. O. Statton, *J. Polym. Sci., C*, **13**, 133 (1966).
53. Handbook of Mathematical Functions, National Bureau of Standards, Applied Mathematics Series No. 55, Section 10.1.11, Washington, D. C., 1964.
54. U. Bonse and M. Hart, in *Small-Angle X-Ray Scattering*, Brumberger, H., Ed., Gordon and Breach, New York, 1967, p. 121.
55. W. E. Danielson, L. Shenfil, and J. W. M. Du Mond, *J. Appl. Phys.*, **23**, 860 (1952).
56. E. W. Fisher, H. Goddar, and G. F. Schmidt, *Kolloid-Z. Z. Polym.*, **226**, 30 (1968).

Received June 23, 1971